Graduate Project Report: Pulse Oximetry Simulation using MCXLab

Wenxin Fang
Student ID:922848311
wxfang@ucdavis.edu

***Abstract*—This project compares three methods for computing the mean path length ratio between two wavelengths using Monte-Carlo simulation (MCXLab). The ratio will then be used to calculate the pulse oxygen level. The current method had low accuracies for pulse oxygen levels lower than 80%. A one-layer model is used to validate the three methods. In addition, a two-layer model is introduced to help study fetal pulse oxygen saturation in the future.**

***Index Terms*—Mean path length ratio, Pulse oxygen saturation, MCXLab**

I. Introduction

Currently, pulse oximetry devices to measure fetal oxygen saturation are under development. Trans-abdominal monitoring is an ideal way to reduce the external influence on the fetus [8]. Pulse oxygen saturation (SpO_2) is the estimation of arterial oxygen saturation (SaO_2) with pulse oximeters. The principle of the pulse oximeter is diffuse optical spectroscopy. By shining light at two wavelengths into the skin and detecting the intensity change from the heart pulsation, SpO_2 can be calculated with the absorbance rate and the total amount of oxygen-bound hemoglobin (HbT) [4]. Analytically, SpO_2 can be calculated by the modified Beer-Lambert Law (mBLL). It relates the absorption of light by the tissue to changes in hemoglobin concentration and the path length traveled by the light. Conventionally, the mean path length ($\langle L \rangle$) or the $\langle L \rangle$ ratio ($\langle \hat{L} \rangle$) between two wavelengths is assumed to be constant [5] over a small range of saturation change. However, it is a function of absorption (μ_a) and reduced scattering (μ_s') coefficients of tissue. The arterial oxygen saturation, SaO_2, is defined as [HbO]/([HbO]+[Hb]), where [HbO] is the concentration of oxy-hemoglobin and [Hb] is the concentration of deoxy-hemoglobin in the arterial blood. During the calibration process, healthy adult volunteers inhale air with lower oxygen content to decrease their SaO_2, and calibration factors derived from the measured signals are then used to correlate with each SaO_2 level [4]. In the experiment, SaO_2 lower than 80% can harm healthy adults, however, an individual's SaO_2 can fall well below 80% before clinical signs. Also, the arterial oxygen saturation can be as low as 40% [3] for a normal fetus. Thus, accuracy for SpO_2 below 80% is significant and could guide vital therapeutic decisions. This project was inspired by the self-calibrated algorithm introduced by Jingyi et. al [7], which used a changing $\langle \hat{L} \rangle$ for different oxygen levels and wavelengths for a single layer model. The result calculated with a self-calibrated $\langle \hat{L} \rangle$ shows comparable accuracies at high SaO_2 levels and outperformed the conventional method (mBLL with a constant $\langle \hat{L} \rangle$) at low SaO_2. In this project, we first validate the self-calibrated algorithm with a one-layer model and then apply it to a two-layer model.

Previous studies have provided fetal SpO_2 estimation with multiple detectors embedded, the RMSE is 6.37% [2]. The estimation from the self-calibrated algorithm has an MAE of 8.37 for SaO_2 lower than 80% [3]. Since they used different error calculations, whether there will be improvements in accuracy remains unknown. However, with the help of this project, the oximeter can significantly reduce the number of detectors and simplify data post-processing.

II. Self-calibrated Algorithm

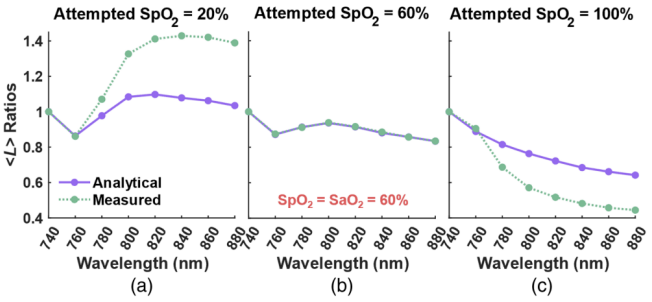

Fig. 1. Process to find the correct SpO_2

From the paper of Jingyi et. al [7], a self-calibrated algorithm has been developed using methods 2 and 3 in the method section. They used 5 different wavelengths and tested them on human free divers. The algorithm generated functions of $\langle \hat{L} \rangle$ with respect to SpO_2.

The measured $\langle \hat{L} \rangle$ is constructed from method 2. They substitute Δ[Hb] with $SpO_2 = \Delta[HbO]/(\Delta[HbO]+\Delta[Hb])$ into equation 1, which makes

$$\langle L \rangle^{\lambda} = \Delta OD^{\lambda}(\Delta[HbO][\epsilon^{\lambda}_{HbO} + (SpO_2^{-1} - 1)\epsilon^{\lambda}_{Hb}])^{-1}$$

$$\langle \hat{L} \rangle^{\lambda}_{\text{measured}}(SpO_2) = \frac{\Delta OD^{\lambda}}{\Delta OD^{\lambda_1}} \frac{(\Delta[HbO][\epsilon^{\lambda_1}_{HbO} + (SpO_2^{-1} - 1)\epsilon^{\lambda_1}_{Hb}])^{-1}}{(\Delta[HbO][\epsilon^{\lambda}_{HbO} + (SpO_2^{-1} - 1)\epsilon^{\lambda}_{Hb}])^{-1}}$$

The analytical $\langle \hat{L} \rangle$ formulation is the same as equations 2 and 3. The estimated SpO_2 is calculated by generating $\langle \hat{L} \rangle$ with respect to wavelengths for all oxygen levels from 1 to 100. Then they used residual squared error (RSS) to determine the

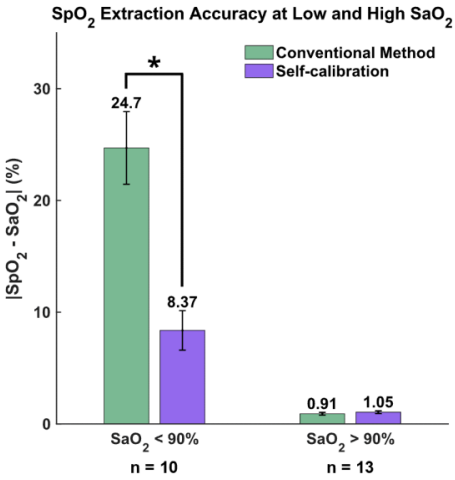

Fig. 2. MAE at low and high saturation level

best $\langle \hat{L} \rangle$. Figure 1 shows the process of finding the correct $\hat{\text{SpO}}_2$. Compared to the traditional method with a constant $\langle \hat{L} \rangle$, Figure 2 shows the improvements in estimation accuracy.

III. Monte-Carlo Simulation

A. General information

We used Monte-Carlo photon simulation (MCXLab) to generate synthetic data [6]. The methods will be explained in detail in the methods section. MCXLab is a native MEX version of MCX for Matlab and GNU Octave. It compiles the entire MCX code into a MEX function which can be called directly inside Matlab or Octave. The input and output files in MCX are replaced by convenient in-memory struct variables in MCXLab, making it easier to use and interact. By default, they compile MCXLab with the support of recording detected photon partial path lengths (L). For simplicity, we keep optical properties other than μ_a unchanged. The photon partial path lengths do not change if we only change the absorbance coefficient μ_a. For each run, if all the parameters stay the same, we will get the same results.

B. Settings

To mimic cardiac pulsations, systolic and diastolic μ_a simulations were performed. We designed a semi-infinite homogeneous medium with SaO_2 at 20%, 40%, 60%, 80% and 100% at two wavelengths (780nm and 850nm). A 3% change from baseline total hemoglobin concentration ([HbT], assumed to be 50μM) due to pulsation was assumed. Reduced scattering μ_s' was considered constant for the whole experiment. The dimensions of the modeled media were set to 100nm for its width, length, and height. A simulated isotropic source with a photon count of 1×10^8 was placed at the center of the modeled tissue surface, and the detector was placed at multiple distances.

C. μ_a calculation

The standard formula to get μ_a is

$$\mu_a = (2.303)e(x \text{ g/liter})/(64,500g \text{ Hb/mole})$$

To explain the formula further, we changed the [HbT] concentration unit to mMolar. Then the formula becomes

$$\mu_a = 2.303 \times (e[\text{HbO}] \times [\text{HbO}] + e[\text{Hb}] \times [\text{Hb}])$$

The extinction coefficient can be found from the literature(citation). For wavelength of 780nm, e[HbO]=710, e[Hb]=1075.44, and for wavelength of 850nm, e[HbO]=1058, e[Hb]=691.32. [HbT]=0.05 mM, [HbO]=$SaO_2 \times$[HbT], [HbO]=(1-SaO_2)$\times$[HbT].

IV. Methods

In this project, we compare 3 different methods to calculate and validate the $\langle L \rangle$ ratio ($\langle \hat{L} \rangle$), which will further be used to estimate the SaO_2.

A. Method 1: Direct calculation with partial path lengths

In MCXLab, they provide functions to calculate detected photon weights and mean path lengths. The formula of mean path length is as follows:

$$\langle L \rangle^\lambda = \frac{\sum(e^{-\mu_a^\lambda L} \times L)}{\sum(e^{-\mu_a^\lambda L})}$$

After calculating the mean path length for the two wavelength and take the ratio we can get

$$\langle \hat{L} \rangle_{\text{direct}} = \frac{\langle L \rangle^{780}}{\langle L \rangle^{850}}$$

B. Method 2: Use the difference of cardiac cycle

If we assume the measured light intensity is solely modulated by the artery blood volume variation during the cardiac cycle, leading to [HbO] and [Hb] at the heart rate (HR) frequency, the change in optical density (ΔOD) can be defined by the mBLL:

$$\begin{aligned} \Delta OD &= \ln(\frac{I_d^\lambda}{I_s^\lambda}) \\ &= \langle L \rangle^\lambda \Delta\mu_a^\lambda \\ &= \langle L \rangle^\lambda (\Delta[\text{HbO}]\epsilon_{\text{HbO}}^\lambda + \Delta[\text{Hb}]\epsilon_{\text{Hb}}^\lambda) \end{aligned} \tag{1}$$

where I_d and I_s are intensities measured at the diastolic and systolic states of the cardiac cycle, respectively; $\Delta\mu_a$ is the change in the absorption coefficient; and ϵ is the extinction coefficient. The intensity is calculated with $I = e^{-\mu_a \times L}$. $\Delta\mu_a = \mu_{a_{systolic}} - \mu_{a_{diastolic}}$.

$$\langle L \rangle^\lambda = \frac{\Delta OD^\lambda}{\Delta\mu_a^\lambda}$$

$$\langle \hat{L} \rangle_{\text{measured}} = \frac{\Delta OD^{780}}{\Delta OD^{850}} \frac{\Delta\mu_a^{850}}{\Delta\mu_a^{780}}$$

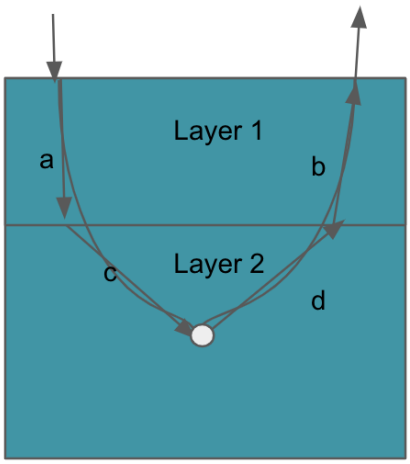

Fig. 3. Two-layer model for a single photon

C. Method 3: Analytical result

The analytical equation of $\langle L \rangle$ in a semi-infinite medium for a reflectance measurement is

$$\begin{aligned} \langle L \rangle^{\lambda}_{\text{analytical}} &\equiv \text{DPF}_{\text{seminf}} \cdot r \\ &= \frac{\sqrt{3\mu_s'^{\lambda}}}{2\sqrt{\mu_a^{\lambda}}} \frac{r\sqrt{3\mu_a^{\lambda}\mu_s'^{\lambda}}}{r\sqrt{3\mu_a^{\lambda}\mu_s'^{\lambda}}+1} \cdot r \\ &= \frac{3}{2} \frac{r^2\mu_s'^{\lambda}}{r\sqrt{3\mu_a^{\lambda}\mu_s'^{\lambda}}+1} \end{aligned} \tag{2}$$

where DPF_{seminf} is the differential pathlength factor in semi-infinite medium, and r is the source-detector distance. μ_s' can be calculated with optical property g and μ_s, where $\mu_s' = (1-g)\mu_s$ [1]. μ_a^{λ} can be substituted by $\mu_a^{\lambda} = [\text{HbO}]\epsilon^{\lambda}_{\text{HbO}} + [\text{Hb}]\epsilon^{\lambda}_{\text{Hb}} = [\text{HbO}][\epsilon^{\lambda}_{\text{HbO}} + (\text{SpO}_2^{-1} - 1)\epsilon^{\lambda}_{\text{Hb}}]$. Then the $\langle \hat{L} \rangle^{\lambda}_{\text{analytical}}$ is a function of SpO_2.

$$\langle \hat{L} \rangle_{\text{analytical}}(\text{SpO}_2) = \frac{\langle L \rangle^{780}_{\text{analytical}}(\mu_a^{\lambda}(\text{SpO}_2))}{\langle L \rangle^{850}_{\text{analytical}}(\mu_a^{\lambda}(\text{SpO}_2))} \tag{3}$$

D. Changes in two-layer model

For the two-layer model, we only used methods 1 and 2. There are also a few changes in the calculation for the two-layer model. Here we take L_1 and L_2 to represent the partial path lengths of each photon in layer one and layer two, where L_1 is the upper layer. With representations in Figure 3, L_1 = a+b, L_2 = c+d. The direct calculation of the mean path length is now:

$$\langle L \rangle^{\lambda} = \frac{\sum(e^{-\mu_{a1}^{\lambda}L_1 - \mu_{a2}^{\lambda}L_2} \times L)}{\sum(e^{-\mu_{a1}^{\lambda}L_1 - \mu_{a2}^{\lambda}L_2})}$$

The intensity calculation also changed to

$$I = e^{-\mu_{a1} \times L_1 - \mu_{a2} \times L_2}$$

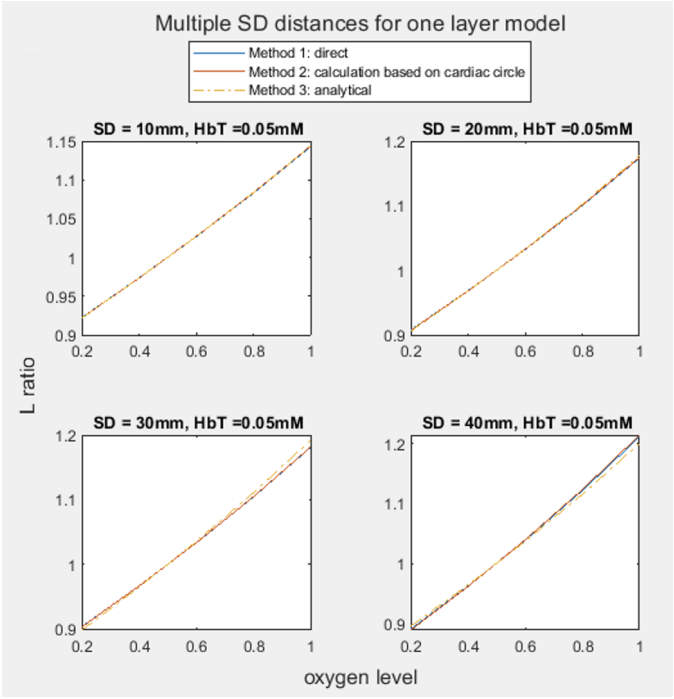

Fig. 4. Multiple SD distances for one-layer model. From the figure, we can see that the change of SD distances will not affect the alignment of the three methods.

V. Result

A. One layer model

The one-layer model is the simplified version with only one-layer of homogeneous medium built using MCXLab. A bunch of photons will depart the sender, traveling through the medium, and finally, some will make it to the surface and be detected by the detector. Since changing μ_a did not change the partial path length generated, I only ran the Monte-Carlo simulation once for all oxygen levels. By doing this, we can save computation cost, energy, and time. The reason why this happens is related to the way developers build MCXLab to run Monte-Carlo simulation.

For real experiments, the distance between the sender and detector may be fixed or difficult to adjust, so it is important to see whether the three methods work over different sender-to-detector (SD) distances. Figure 4 shows that with different SD distances, the performance of the three methods is stable. Also, the HbT concentration has a certain range since the experiment can be done on the fore-arm and forehead, it is vital to see if the model can work within the range of our HbT concentration. From Figure 5, we can see that generally, the three methods align with each other, though there are some anomalies with extremely small or large HbT concentrations. During the real-life experiment, we should pay more attention to the HbT concentration.

B. Two layer model

For two-layer models, we currently set one layer with fixed μ_a and the other with the diastolic and systolic states to

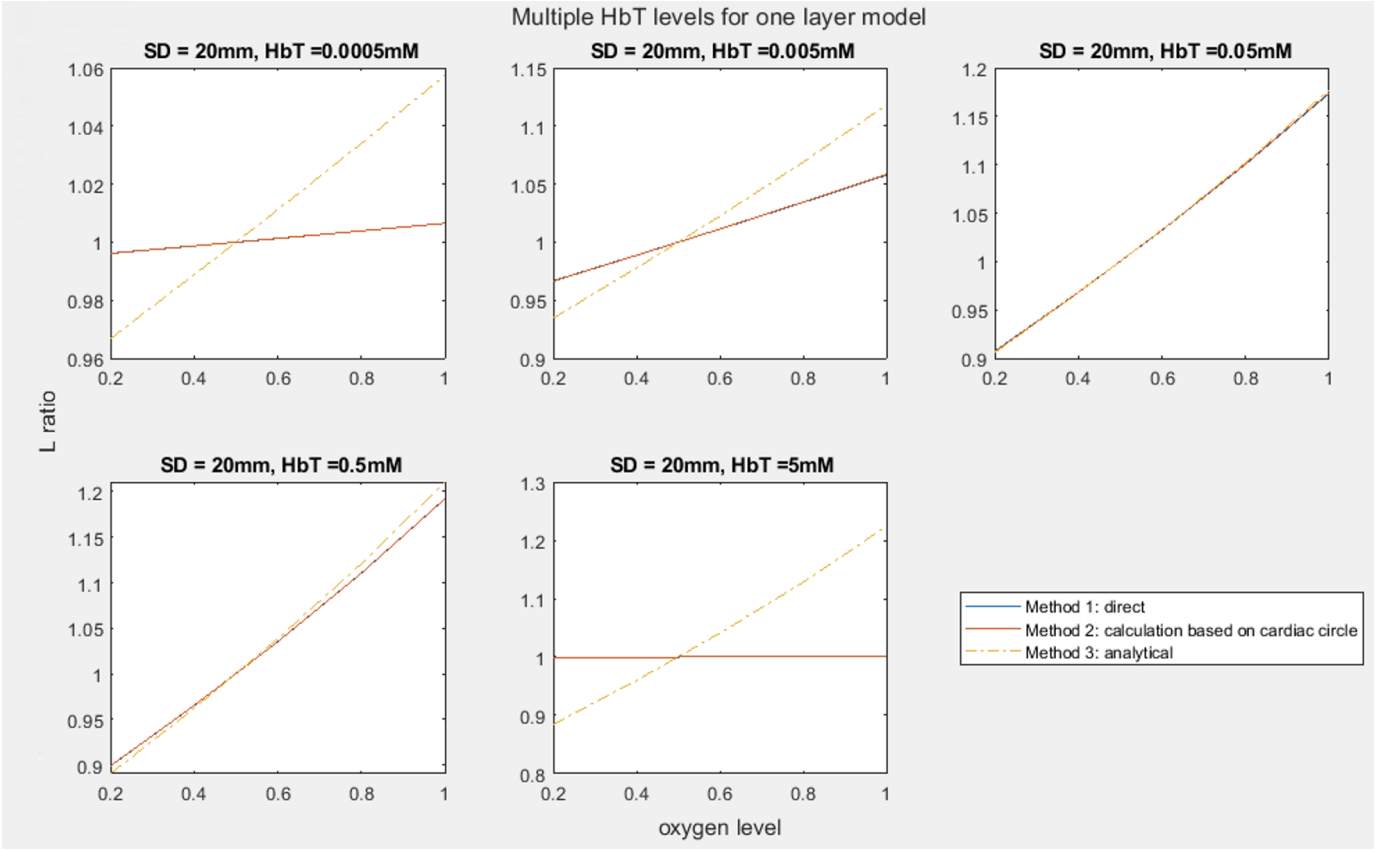

Fig. 5. Multiple HbT concentrations with SD = 20mm for one-layer model. The figure shows that within a small range, the three methods align. For small and large HbT concentrations, the analytical approach can not align with the other two methods.

see if the results align between these two methods, because the experimental data provides the intensities, and we hope to accurately estimate oxygen level based on intensities. I calculated the $\langle \hat{L} \rangle$ using methods 1 and 2 because method 3 does not provide a multi-layer model. First, I calculated the two-layer model with method 1, from which I will get two curves representing the ratio for layer 1 and layer 2; the x-axis is also the oxygen level. Second, I use method 2 to calculate the ratio for layer 1 or layer 2. Results were conducted with multiple depths, multiple sender-to-detector distances, and multiple HbT concentrations. From the result, we can see that if we keep μ_a in layer 2 unchanged, the measured ratio of layer 1 is almost the same as the direct one. And if we keep μ_a in layer 1 unchanged, the results generally align within a certain range of thickness, SD distances, and HbT concentration.

For Figures 6, 7, and 8, the above figure is the layer 2 estimates and the figure below is the layer 1 estimates. We take the thicknesses of 20, 30, and 40mm to test the performance. Thickness will influence layer 2 more since, as layer 1 gets thicker, the photon numbers in layer 2 will be reduced. As shown in Figure 6, the performance of both layer estimates is satisfactory. Similar to the one-layer model, we also tried multiple SD distances (10, 20, 30mm), as shown in Figures 7 and 8. Layer 1 estimates maintain the performance, and layer 2 estimates are good under thicknesses of 20mm and 40mm. Since layer 1 estimates show excellent robustness and we mainly focus on the performance of layer 2. Figure 9 shows the performance of layer 2 estimates under the same HbT concentration range as in the one-layer model. Compared to the one-layer model, the two-layer model had a tighter range of HbT concentration for the two methods to align.

After validating the self-calibrated method, the next step is to use the experiment data. Only methods 1 and 2 will be used. First, we should generate the benchmark using the same optical properties and parameters using method 1 in MCXLab. This $\langle \hat{L} \rangle_{\text{benchmark}}$ will then be compared with the ratios calculated from the real data. For experiment data, we only have intensity I for both diastolic and systolic states. Then plug in all oxygen levels from 1 to 100 using method 2 to get a plot of $\langle \hat{L} \rangle_{\text{measured}}$. Plot $\langle \hat{L} \rangle_{\text{benchmark}}$ in the same figure. The x-axis of the crossing dot will be our estimates of SpO_2.

VI. Conclusion

To conclude, this project validates the self-calibrated algorithm for a one-layer model and tests the algorithm on a two-layer model. The next step is to validate using real experiment data and ultimately it will be helpful to further study the fetal pulse oximetry.

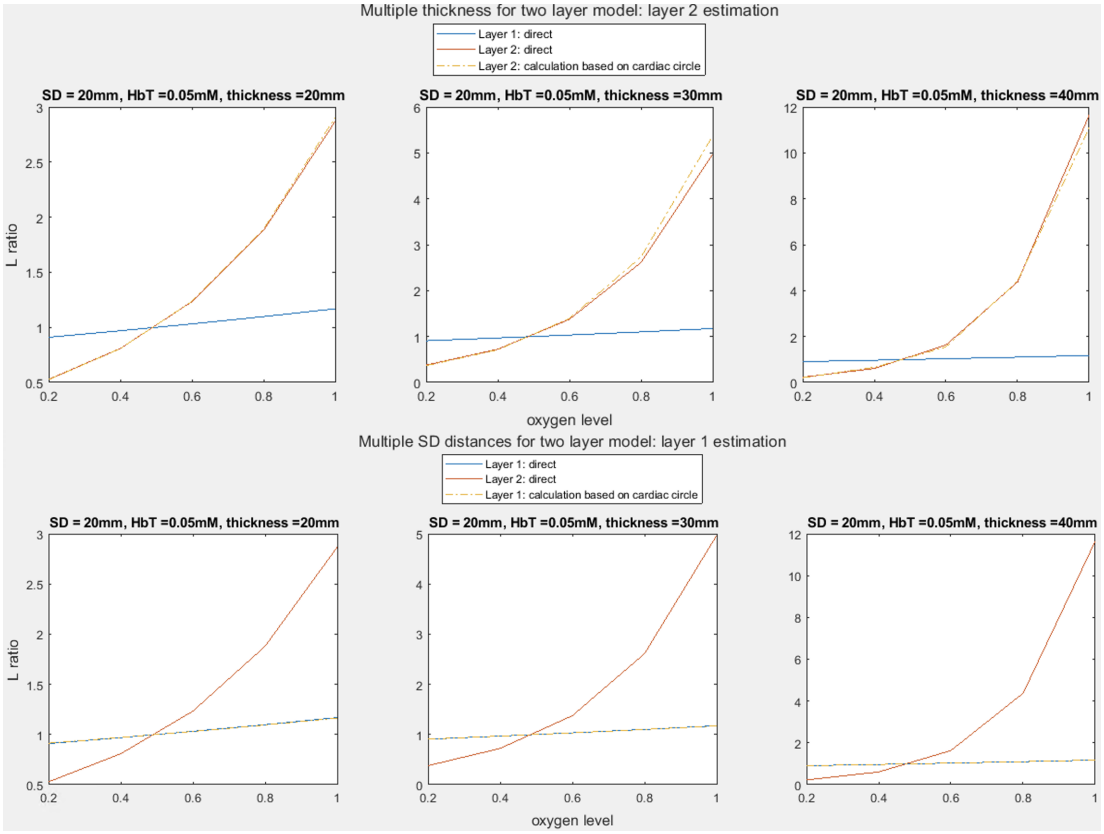

Fig. 6. Multiple thickness with SD = 20mm for two-layer model. The thickness represents the depth of layer 1, which is also the layer closer to the medium surface.

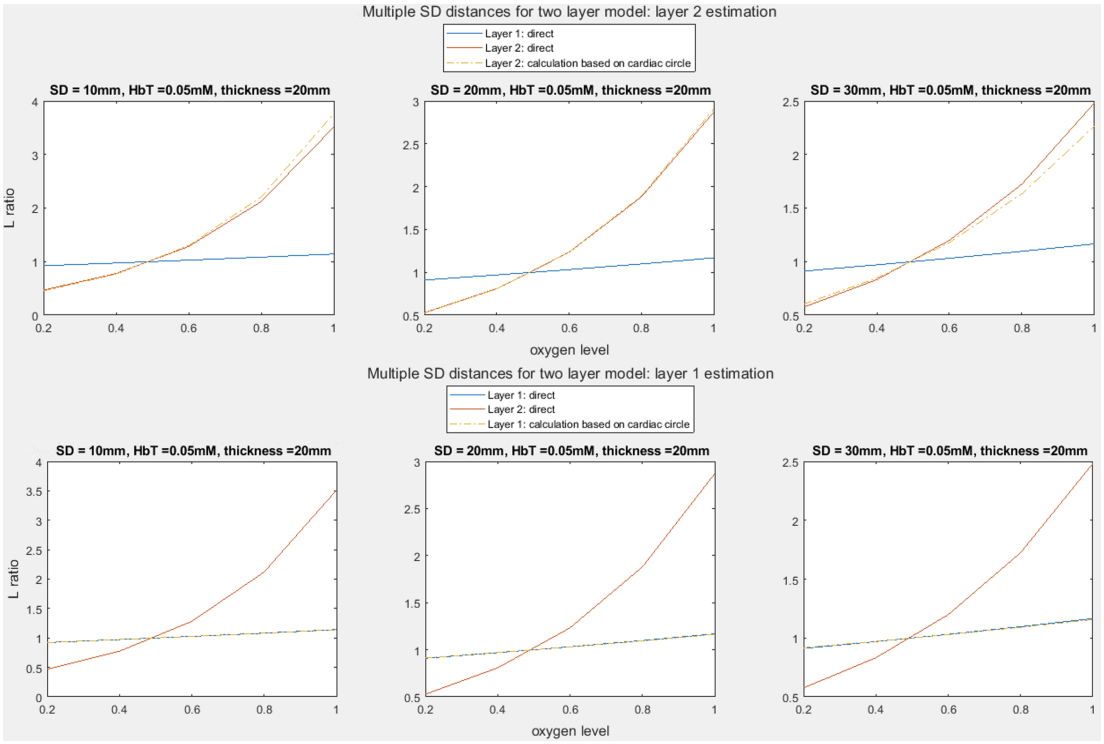

Fig. 7. Multiple SD distances with thickness = 20mm for two-layer model.

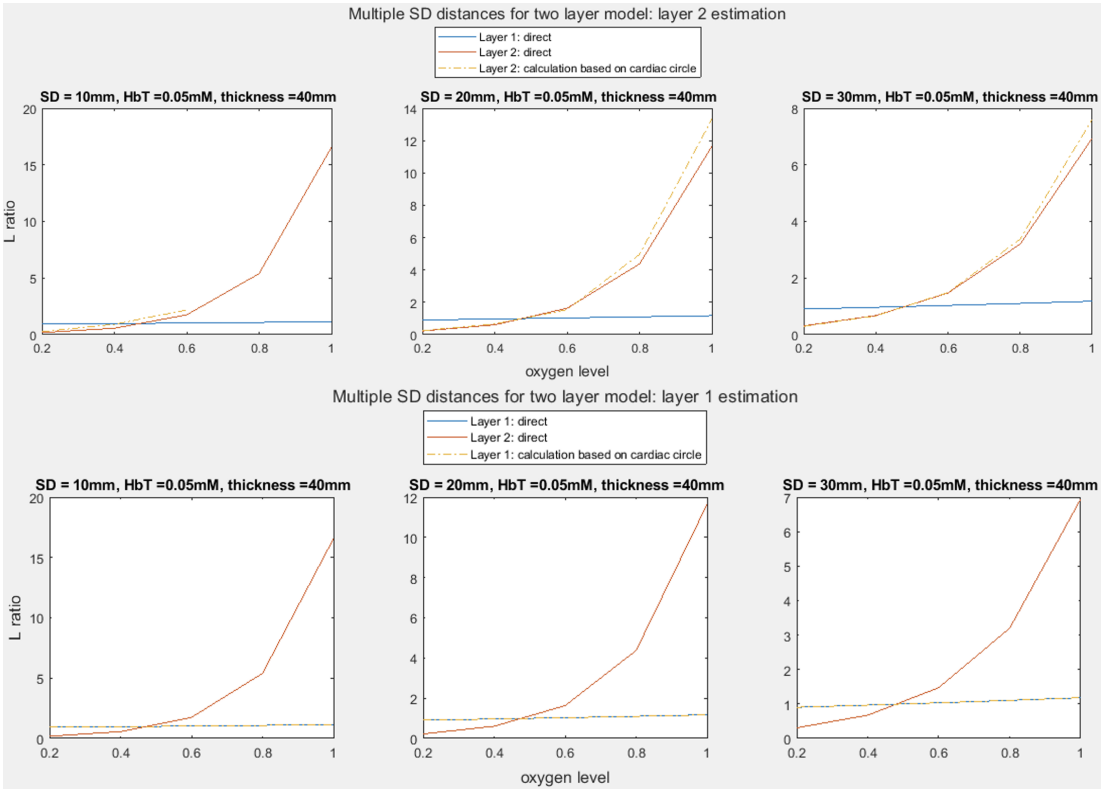

Fig. 8. Multiple SD distances with thickness = 40mm for two-layer model.

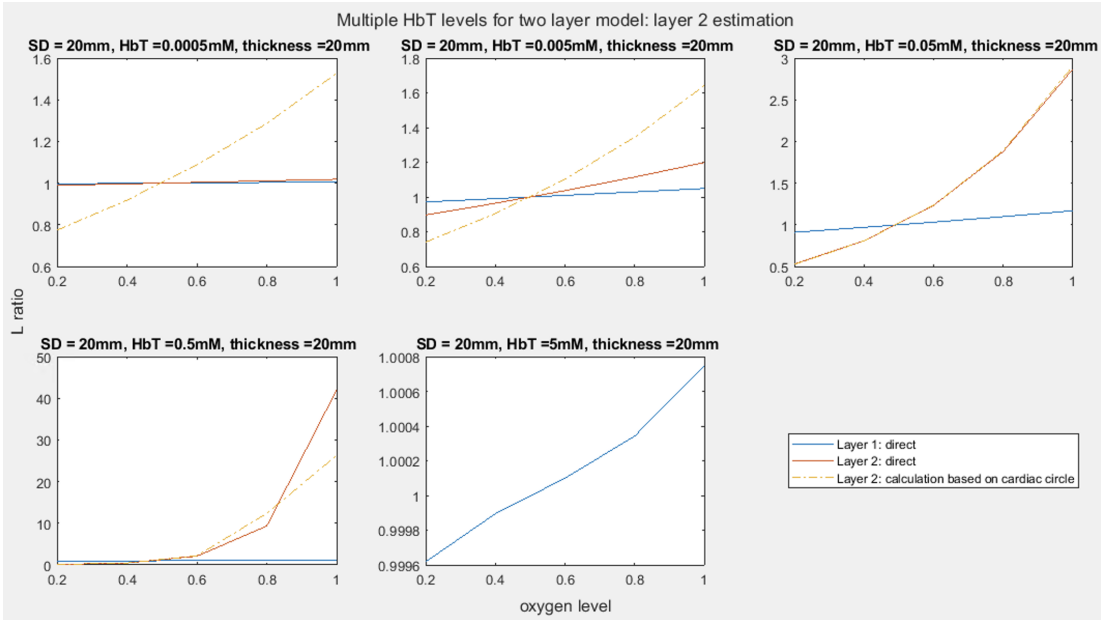

Fig. 9. Multiple HbT concentrations for two-layer model

REFERENCES

[1] Dimofte, A., Finlay, J. C., Zhu, T. C. (2005). A method for the determination of the absorption and scattering properties interstitially in turbid media. Physics in medicine and biology, 50(10), 2291–2311. https://doi.org/10.1088/0031-9155/50/10/008

[2] Fong, D. D., Yamashiro, K. J., Vali, K., Galganski, L. A., Thies, J., Moeinzadeh, R., Pivetti, C., Knoesen, A., Srinivasan, V. J., Hedriana, H. L., Farmer, D. L., Johnson, M. A., Ghiasi, S. (2021). Design and In Vivo Evaluation of a Non-Invasive Transabdominal Fetal Pulse Oximeter. IEEE transactions on bio-medical engineering, 68(1), 256–266. https://doi.org/10.1109/TBME.2020.3000977

[3] F. C. Battaglia and G. Meschia, An Introduction to Fetal Physiology, Academic, Orlando (1986).

[4] J. E. Sinex, "Pulse oximetry: principles and limitations," Am. J. Emerg. Med. 17(1), 59–66 (1999).

[5] L. Kocsis, P. Herman, and A. Eke, "The modified Beer–Lambert law revisited," Phys. Med. Biol. 51(5), N91–N98 (2006).

[6] Q. Fang and D. A. Boas, "Monte Carlo simulation of photon migration in 3D turbid media accelerated by graphics processing units," Opt. Express 17(22), 20178 (2009).

[7] Wu, J., McKnight, J. C., Bønnelycke, E. S., Bosco, G., Giacon, T. A., Kainerstorfer, J. M. (2023). Self-calibrated pulse oximetry algorithm based on photon pathlength change and the application in human freedivers. Journal of biomedical optics, 28(11), 115002. https://doi.org/10.1117/1.JBO.28.11.115002

[8] Zourabian, A., Siegel, A., Chance, B., Ramanujan, N., Rode, M., Boas, D. A. (2000). Trans-abdominal monitoring of fetal arterial blood oxygenation using pulse oximetry. Journal of biomedical optics, 5(4), 391–405. https://doi.org/10.1117/1.1289359